ROYAL SOCIETY OF CHEMISTRY

PAPER

Check for updates

Enhanced ketonic decarboxylation of fatty acids using vanadia-modified nickel on zirconia catalysts†

Sibongile Pikoli, [ID] Avela Kunene and Banothile C. E. Makhubela [ID] *

Ketonic decarboxylation of carboxylic acids over ZrO_2-modified catalysts has proven highly effective in yielding ketones and bio-hydrocarbons – key intermediates in biofuel and chemical manufacturing. However, most studies have focused on carboxylic acids with $C_1–C_4$ chains. This study explores the effect of modifying ZrO_2 catalysts with cost-effective transition metals to enhance the cross-ketonization of triglyceride-derived C_{18} fatty acids with acetic acid to the C_{19} fatty ketone, nonadecanone. Further deoxygenation of nonadecanone – with ~18–23% carbon retention ($C_{12}–C_{18}$) – signifying preservation of the green diesel energy density was achieved. We introduce an *in situ* hydrogen generation strategy *via* formic acid decomposition, which preferentially hydrogenates tall oil fatty acid (TOFA) into stearic acid, significantly improving cross-ketonization. This approach afforded up to 93% conversion, with a catalyst turnover frequency (TOF) of 69 h^{-1}, yielding 64% nonadecanone and ~20% green diesel-range bio-hydrocarbons ($C_{12}–C_{18}$) in a stirred-batch reactor (SBR) system using 10 wt% Ni/ZrO_2 at 350 °C for 5 h. The inherently low bio-hydrocarbon selectivity from unsaturated TOFA feedstock was improved by applying 10 bar of hydrogen pressure, coupled with hydrogen from formic acid decomposition, leading to a 1.5-fold increase in bio-hydrocarbon yield – confirming a saturated fatty acid-favoured cross-ketonization pathway. Furthermore, vanadia (V_2O_5) modification of the Ni/ZrO_2 catalyst enhanced bio-hydrocarbon selectivity (~45%) by facilitating nonadecanone deoxygenation. These findings highlight the role of acid–base tuning in Ni/ZrO_2 catalysts, demonstrating that vanadia doping effectively promotes ketonization and deoxygenation of fatty acids, advancing sustainable green diesel and biochemical (nonadecanone) production.

1. Introduction

Renewable biomass has shown significant potential as a sustainable alternative energy source. This is highlighted by profitable sectors that focus on transforming biomass into renewable energy and bulk chemicals.[1,2] Triglycerides extracted from vegetable oils and animal fats are a notable example, being both economical and environmentally benign.[3] The production of biodiesel (fatty acid methyl esters) from the transesterification of triglycerides has been investigated extensively as a potential fuel substitute for petroleum-based fuel.[4,5] However, the application of this fuel type is limited by its low heat value, poor oxidation stability, and engine corrosion due to the high oxygen content, making oxygen removal a necessary step.[6,7]

Research Centre for Synthesis and Catalysis, Department of Chemical Science, University of Johannesburg, Auckland Park, 2006, South Africa. E-mail: bmakhubela@uj.ac.za

† Electronic supplementary information (ESI) available. See DOI: https://doi.org/10.1039/d4se01836b

Hydrodeoxygenation,[8] decarboxylation,[9] and decarbonylation[10] are standard deoxygenation methods that eliminate oxygen in the form of water, carbon dioxide, and carbon monoxide, respectively. Despite their strong potential for renewable diesel production, these methods have significant drawbacks: hydrodeoxygenation requires excessive hydrogen pressure and catalysts comprised of noble metals and sulfided materials – the latter often introducing unwanted sulfur into the resultant bio-hydrocarbon, thereby compromising fuel standards.[11–13] Decarboxylation and decarbonylation promote carbon–carbon (C–C) bond cleavage, which results in carbon loss and reduced fuel energy density.[14,15]

Ketonic decarboxylation (ketonization) is a highly efficient, eco-friendly alternative that condenses two molecules of carboxylic acids *via* C–C coupling, removing oxygen as carbon dioxide and water.[16] This deoxygenation pathway offers several advantages, including enhanced carbon retention, reduced energy consumption, and minimized dependency on external reagents such as solvents.[17] The ketone is formed through a reaction pathway involving hydrogen abstraction at the α-C position of the carboxylic acid as a first step before subsequent transformations. This reaction leverages the electron-

withdrawing nature of the carboxylic acid, while the ketone product may exhibit electron-donating and electron-withdrawing behaviour depending on its molecular context.[18]

Short-chain carboxylic acids are commonly utilized in ketonic decarboxylation reactions—such as the formation of acetone from the self-ketonization of acetic acid.[19,20] Fatty acids from forestry and waste cooking oil present a more sustainable approach for producing diesel-range fuels (C_{12}–C_{18}) and lube-base oleochemicals.[21] An example is tall oil fatty acid (TOFA), a non-edible, abundant, and affordable raw material made up of C_{18} fatty acids, the most common in nature.[22,23] This fatty acid is obtained by distilling crude tall oil and is the third-largest chemical byproduct produced by the pulp and paper industry.[24,25] With a global market of USD 1 billion in 2020, TOFA is both economically and environmentally appealing.[26]

Although the deoxygenation of tall oil fatty acid has been studied to some degree, the primary reaction pathway under high hydrogen pressure has been decarboxylation, leading to the formation of C_{n-1} bio-hydrocarbons. Mäki-Arvela et al. reported the deoxygenation of TOFA over Pd/C, which resulted in 59% conversion and 91% heptadecane selectivity at 350 °C in 5.5 hours using 100% H_2.[27] Jenistova and colleagues also reported the effect of hydrogen pressure on the hydro-deoxygenation of TOFA where the highest conversion (99%) with 97% heptadecane selectivity was observed at 300 °C/6 h over 30 bar H_2.[28] When comparing the conversion of TOFA with that of stearic acid under the same reaction conditions, it could be seen that highly saturated fatty acids are more prone to deoxygenation than unsaturated compounds. This phenomenon is attributed to catalyst deactivation caused by double bonds in the feedstock. Lee et al. reported a similar observation in the ketonization of C_{18} fatty acids, noting that increased feedstock unsaturation promoted catalyst deactivation. This is due to dienes and methyl ketones forming, likely resulting from the McLafferty rearrangement.[21] Considering that industrial feedstock such as tall oil and waste cooking oil are highly unsaturated, a hydrogenation step may be crucial in obtaining the deoxygenated bio-hydrocarbon.[29]

Ketonization is catalyzed by metal oxides containing surface acid–base properties and oxygen vacancies and proceeds without molecular hydrogen. Notable catalysts include well-researched amphoteric metal oxides like TiO_2 and ZrO_2, which have high lattice energy and excellent ketonization ability.[30,31] These mesoporous materials can be promoted using effective Ru, Pt, and Pd metals. However, the costs associated with noble metals can be limiting to the future development of industrial-scale fatty acid deoxygenation processes.[32,33] Ni is a suitable alternative as an active metal due to its abundance, low cost, and strong hydrogen activation capacity, displaying similar properties to Pd or Pt in C–C and C–H bond cleavage. The performance of Ni-based catalysts can be enhanced by incorporating a promoter metal, which helps optimize the deoxygenation rate, improve product selectivity, and enhance catalyst durability. Furthermore, bimetallic systems can adapt the crystal plane structure of the catalyst to slow down carbon deposition, enhance hydrophobicity, and reduce coking.[34,35] Ni catalysts are effective despite being susceptible to coking due to

their acidic sites. Introducing a promoter metal with lower acidity can enhance the catalyst performance.[36]

Herein, Ni supported on ZrO_2 (Ni/ZrO_2) and vanadia-promoted Ni/ZrO_2 catalysts were prepared and applied in the ketonic decarboxylation of lipid biomass. Vanadium(v) oxide (V_2O_5) is a cost-effective, thermally stable, and sulfur-resistant material that has demonstrated its value in industrial catalytic applications.[37–41] The catalysts, reported herein, were prepared using hydrothermal techniques, with crystal morphology and surface chemistry reported.

Formic acid was employed as a hydrogen donor to partially saturate the feedstock and enhance hydrogen availability, thereby mitigating catalyst deactivation. In tandem with hydrodeoxygenation or decarbonylation–hydrogenation, the one-pot ketonization process offers a promising route for producing energy-dense green diesel-range bio-hydrocarbons. However, its optimization is crucial due to the inherent challenges associated with this method.[42]

Refining the deoxygenation process of raw feedstock requires fine-tuning the catalyst and reaction conditions. The study aimed to determine the optimal conditions for deoxygenating TOFA and other lipid-based feedstocks through cross-ketonization with acetic acid, producing ketones that are subsequently deoxygenated to yield bio-hydrocarbons with carbon numbers corresponding to the original feedstock. Beyond fuel production, this method generated valuable intermediates, including (1) nonadecanone, the primary cross-ketonization product between C_{18} fatty acids and acetic acid, (2) acetone, which is produced selectively from a self-ketonization of the inexpensive acetic acid if used in excess, (3) penta-triacontanone, which can be obtained when excess stearic acid-based feedstocks are present.[42] The findings in this study highlight the critical role of feedstock selection and catalyst design in influencing product distribution and guiding keto-nization reaction pathways.

2. Experimental

2.1. Catalyst preparation

Nanomaterials including nickel oxide (NiO), zirconia (ZrO_2), nickel supported on zirconia (Ni/ZrO_2), and vanadia-promoted nickel supported on zirconia (V–Ni/ZrO_2) were synthesized to investigate the impact of ZrO_2-supported nickel nanocrystals and vanadia-promoted Ni/ZrO_2 catalysts on the ketonic decarboxylation of fatty acid feedstocks. Ni(NO$_3$)$_2$·6H$_2$O (98.0%), ZrOCl$_2$·8H$_2$O (≥99.5%), and NH$_4$VO$_3$ (≥99.0%) were purchased from Sigma Aldrich. The nickel oxide powder and the zirconia support were synthesized using self-assembly and co-precipitation methods.[43,44] The Ni-based catalysts (Ni/ZrO_2 and V–Ni/ZrO_2) were prepared via the wetness impregnation method.[37,45] For Ni/ZrO_2, Ni(NO$_3$)$_2$·6H$_2$O was added to a solution of ZrO_2 in distilled water to make up 10 wt% of Ni followed by stirring at room temperature for one hour. The solvent was then removed using a rotary evaporator. In an oven at 110 °C, the precipitant was dried overnight and calcined at 400 °C, over 6 hours (2 °C min^{-1} ramp). To prepare the vanadia-promoted catalyst (2 wt% V → 8 wt% Ni), a specific amount of NH$_4$VO$_3$ and

$Ni(NO_3)_2 \cdot 6H_2O$ was added to a solution of ZrO_2 in water, after which the salt mixture was stirred at room temperature (RT) for 4 h. The precipitate was recovered under vacuum and then dried in an oven at 80 °C for 24 hours. The solid product underwent a 6 h calcination process with a ramp rate of 2 °C min^{-1}. All calcination processes were conducted under oxidative conditions in the presence of air.

2.2. Catalyst characterization

2.2.1. Inductively coupled plasma-optical emission spectroscopy (ICP-OES).
The metal loading on the support surface was quantified using ICP-OES on a SPECTRO ARCOS instrument.

2.2.2. N$_2$-adsorption/desorption isotherm.
Following an overnight degassing process at 250 °C, the materials' surface areas and porosities were analyzed on a Micrometrics ASAP 2460 at a temperature of −196 °C. The Brauner–Emmet–Teller method (BET) and the Barrett–Joyner–Halenda (BJH) approach were used to determine the surface area and pore-size measurements.[46]

2.2.3 X-ray powder diffraction (XRD).
A PANalytical X'Pert Pro powder diffractometer (X-ray radiation source: Cu Kα ($k = 0.15405$ nm) tube) was used to analyze the metal oxides' diffraction patterns. The results were processed on the ICDD PDF-4+ 2019 database using the High Score (Plus) program. The acquired data were subsequently applied to calculate the crystallite size using Miller indices (hkl) and the Deb–Scherrer equation.[47]

2.2.4 Scanning electron microscopy (SEM).
A TESCAN VEGA 3 LMH (20 kV accelerating voltage) was used to obtain and analyze microscopic images of the porous materials after the samples had been coated with a carbon source using the Agar Turbo Carbon coater. The elemental composition and distribution of the materials were studied using energy dispersive spectroscopy (EDS) and an Oxford secondary detector (SED) with the Aztec analytic tool.

2.2.5. Hydrogen temperature programmed reduction (H$_2$-TPR) and ammonia temperature-programmed desorption (NH$_3$-TPD).
The hydrogen reduction properties of ZrO_2, Ni/ZrO_2, and $V–Ni/ZrO_2$ were evaluated on a Micrometrics 3 Flex, MicroActive Version 5.02. Using the AutoChem II 2920 Plus V5.03 chemisorption analyzer, ammonia temperature-programmed desorption (NH$_3$-TPD) revealed the acidity of the prepared materials.

2.2.6. X-ray photoelectron spectroscopy (XPS).
The electronic and surface states of the oxidic compounds were examined using X-ray photoelectron spectroscopy. Using the Al K (alpha) excitation source (15 mA, 0.15 eV), these parameters were examined on an AXIS Supra+, and the data were processed with the CasaXPS software (version 2.3.22).

2.3. Fatty acid ketonic decarboxylation

The catalyzed ketonization reactions were performed in a batch reactor (20 mL) using a PI-controlled band heater. In a typical reaction, the reactor was charged with 0.87 mmol of TOFA, 1.80 mmol acetic acid, 10 mg of Ni/ZrO$_2$, and 2.50 mmol of formic acid in 3 mL n-hexane. The temperature and time ranges for the reactions were 250–350 °C and 1–5 hours, respectively (Scheme 1). At the end of each reaction cycle, the reactor was quenched in cold water, and the products were recovered and separated using a centrifuge. The liquid products were then diluted with hexane or dichloromethane for analysis. Feedstock raw materials such as TOFA and dehydrated castor oil fatty acid (DCOFA) were supplied by AECI. Palm oil (PO) and waste cooking oil (WCO) were obtained from local Johannesburg markets. Biodiesel was synthesized via the transesterification of WCO (Fig. S1 and S2†).[48,49]

A gas chromatograph fitted with a flame ionization detector (PerkinElmer Claurus 580) was used to quantify the liquid products from the deoxygenation reactions. The products were quantified and identified using the Van den Dool and Kratz equation[50] (eqn (1)), peak regions, and known concentrations of the original feed. The conversion, yield, and selectivity were calculated using decane as an internal reference standard (eqn (2)–(4)). The turnover frequency was calculated as the moles of reactant converted per mole of accessible Ni over a unit of time (eqn (5)). Chemisorption studies have not yet been conducted; therefore, the active sites on the catalyst surface were estimated using the PXRD-derived crystallite size of NiO.[51–53]

$$RI = 100n + 100\frac{(t_x - t_n)}{(t(n+1) - t_n)} \tag{1}$$

where n = lowest number of reference alkanes, t_x = retention time of the compound, t_{n+1} = retention time of the reference alkane eluting after the compound, t_n = retention time of the reference alkane eluting before the compound.

$$Conversion~(\%) = \frac{(moles~of~fatty~acid~in~feed - moles~of~fatty~acid~in~product)}{(moles~of~fatty~acid~in~feed)} \times 100 \tag{2}$$

$$Yield~(\%) = \frac{(moles~of~product)}{(moles~of~fatty~acid~in~feed - moles~of~fatty~acid~in~products)} \times 100 \tag{3}$$
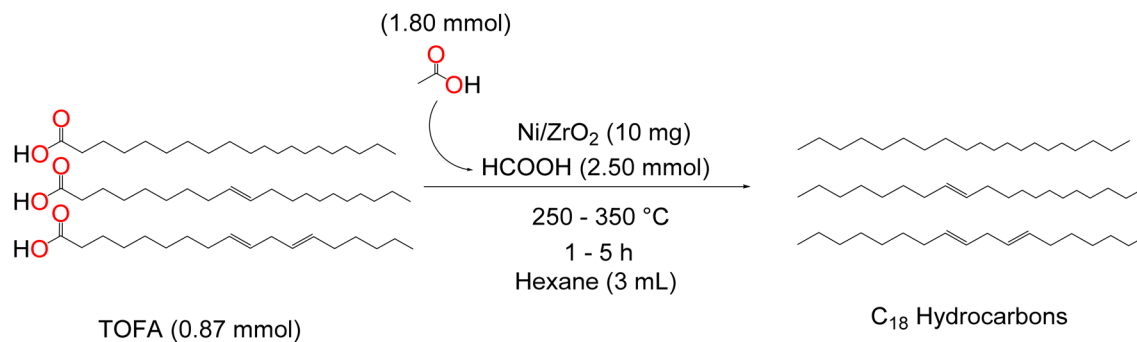
Scheme 1 Catalyzed ketonic decarboxylation of fatty acids over Ni/ZrO$_2$.

$$\text{Selectivity } (\%) = \frac{(\text{moles of desired product})}{(\text{moles of all product})} \times 100 \quad (4)$$

$$\text{TOF } (h^{-1}) = \frac{(\text{moles of fatty acid feed converted})}{(\text{moles of metal} \times \text{dispersion} \times \text{reaction time})} \quad (5)$$

3.   Results and discussion

3.1.   Catalyst properties

Utilizing surface analytical methods like BET, PXRD, SEM-EDS, H$_2$-TPR, NH$_3$-TPD, and XPS, the effect of adding the active nickel phase and vanadia promoter on the crystalline structure and surface chemistry of the zirconia support was assessed.

Minimal changes in the specific surface area and pore volume of the zirconia support were observed following Ni impregnation (Fig. 1a). Adding vanadia to the catalyst system decreased the pore size to 22 nm, indicating alterations in the textural properties and the potential formation of new phases, which affected both the surface area and porosity.

The XRD pattern of ZrO$_2$ displayed a predominant mono-clinic crystal phase with traces of a tetragonal crystalline phase (Fig. 1b). A new peak, attributed to the strongest peak of the NiO active phase, that is seen at 43.4° on the 200-lattice plane of

NiO/ZrO$_2$, confirmed successful impregnation.[17] In the V-modified catalyst, diffraction peaks attributed to V$_2$O$_5$ could not be distinguished, and a broadening of the NiO crystalline peak (42.8°) suggests an improved active phase dispersion.[39] This is evident from the decrease in crystallite size (Table 1), from 9.0 nm for Ni/ZrO$_2$ to 5.3 nm for V–Ni/ZrO$_2$, indicating that vanadia minimizes Ni agglomeration and promotes uniform distribution of the active species. The improved crystallinity of the Ni/ZrO$_2$ diffraction peaks and enhanced peak separation can be attributed to incorporating vanadia species (V^{5+}) into the catalyst lattice.[54]

SEM images depict an aggregation of crushed angular particles, which retained their texture even after impregnation with the active metals (Fig. 2). The active phase dispersion and elemental composition of ZrO$_2$, Ni/ZrO$_2$, and V–Ni/ZrO$_2$ confirmed a uniform Ni distribution, with approximately 13 wt% and 9.3 wt% Ni loading, similar to the ICP-OES, which yielded values of 10 wt% and 8 wt% Ni loading. Vanadium oxide was also identified, albeit in minimal amounts (0.3 wt%), explained by the low mass loading and effective impregnation of vanadium (<2 wt%) in the catalyst system.

The temperature-programmed hydrogen-reduction (H$_2$-TPR) of ZrO$_2$ in the temperature range (25–800 °C) displayed two low-intensity reduction peaks at 412.1 °C and 632.9 °C, which are attributed to hydrogen uptake on the zirconia surface since the
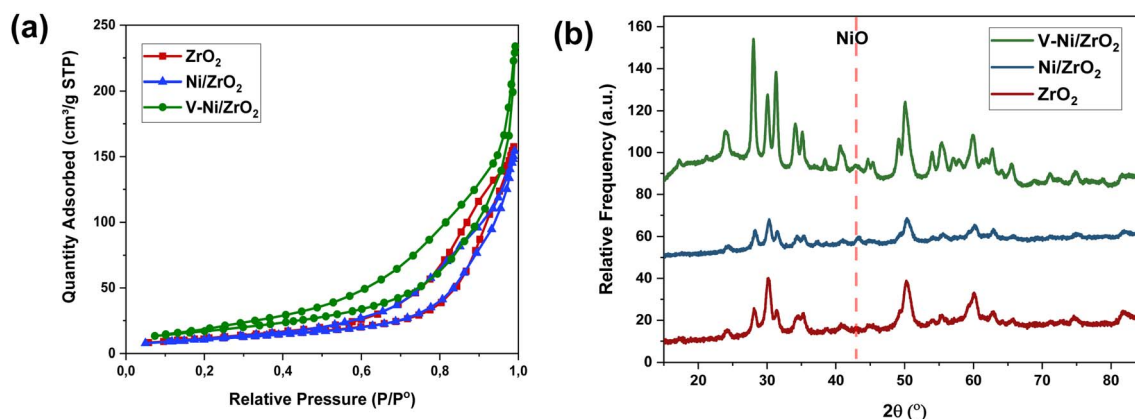

Fig. 1 (a) BET graphs of ZrO$_2$, Ni/ZrO$_2$, and V–Ni/ZrO$_2$ in the P/P^0 range 0.05–0.99; (b) stacked PXRD patterns for zirconia and its Ni-derived catalysts (Ni/ZrO$_2$ and V–Ni/ZrO$_2$).

Table 1 Surface properties of the metal oxide catalysts

Catalyst	[a]N loading	[a]V loading	Specific surface area ($m^2\ g^{-1}$)	Pore size (nm)	[b]Crystallite size	[c]TEM particle size
ZrO_2	—	—	40	24	8.1 (±5.3)	17.4 (±3.9)
Ni/ZrO_2	9.7	—	40	24	9.0 (±3.2)	16.2 (±3.1) 11.7[d]
$V–Ni/ZrO_2$	7.5	1.5	63	22	5.3 (±2.6)	15.1 (±7.3) 5.9[d]

[a] Based on ICP-OES. [b] Based on PXRD data. [c] Based on TEM images (Fig. S3). [d] Based on NiO(200) crystallite size calculation.
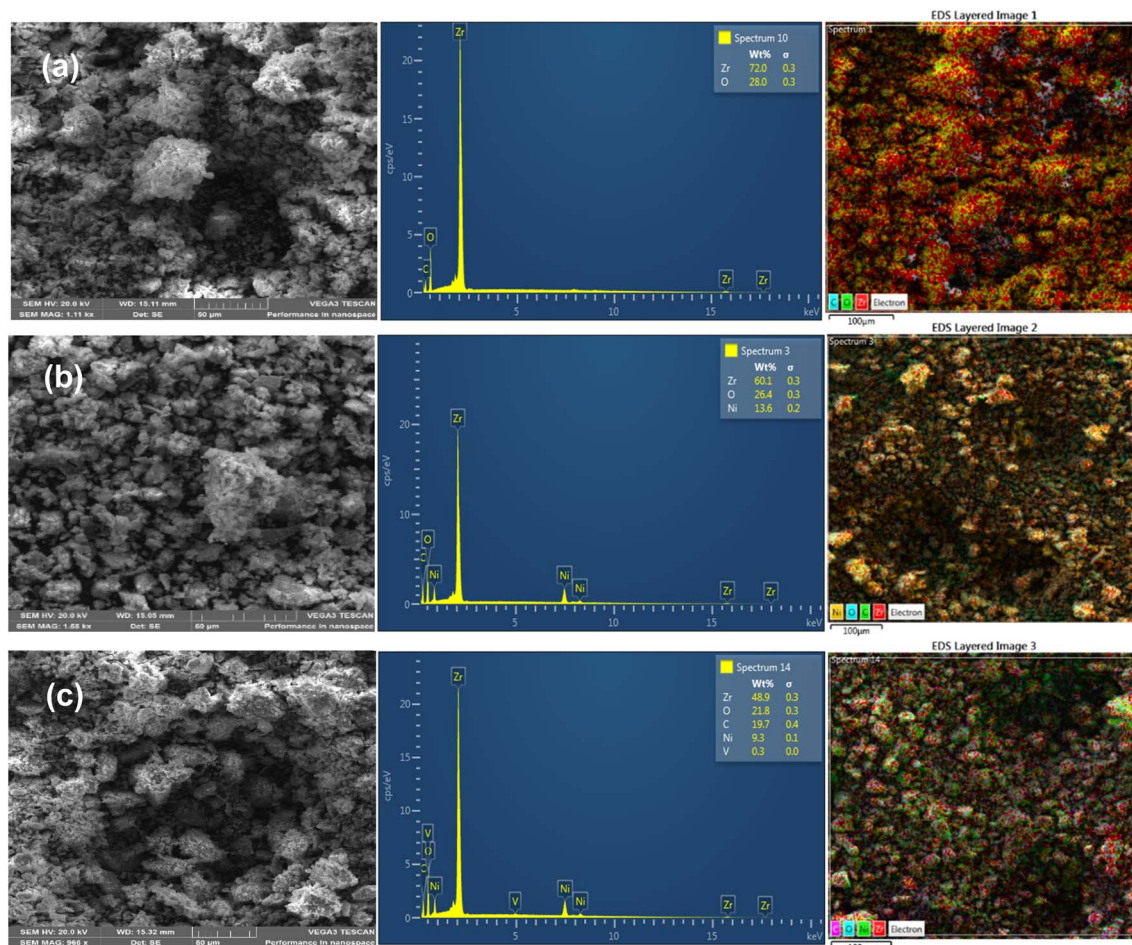
Fig. 2 SEM images and elemental mapping of the metal oxide catalysts: (a) ZrO_2, (b) Ni/ZrO_2 and (c) $V–Ni/ZrO_2$.

support material is not easily reduced (Fig. 3a). For Ni/ZrO_2, the peaks at 338.6 °C and 437.6 °C indicate weak to medium metal-to-support interactions due to NiO particles adsorbed on the support surface. In contrast, the higher temperature peak suggests strong interactions, representing the reduction of NiO nanoparticles embedded within the support structure. The V-promoted catalyst depicted three shoulder peaks at 290.9 °C, 348.6 °C, and 414.4 °C ascribed to the hydrogen reduction of weakly bound NiO particles, the surface adsorbed NiO nano-particles, and the NiO material embedded into the support, respectively.[55] The increased peak intensity for NiO reduction

above 400 °C suggests that the V promoter strengthens the metal-to-support interactions between NiO and ZrO_2, resulting in better dispersion of the active species, higher hydrogen uptake, and a lower reduction temperature.

The ammonia temperature-programmed desorption illustrating the surface acidity of ZrO_2, Ni/ZrO_2, and $V–Ni/ZrO_2$ is displayed in Fig. 3b from 150 °C to 600 °C. Weak acid sites on the support and Ni/ZrO_2 catalyst were observed at ~150 °C assigned to the zirconia surface acidity.[56] Desorption peaks over Ni/ZrO_2 in the weak to medium acidity (at 298 °C) and strong acidity (at ~620 °C) regions are attributed to weak acid sites of
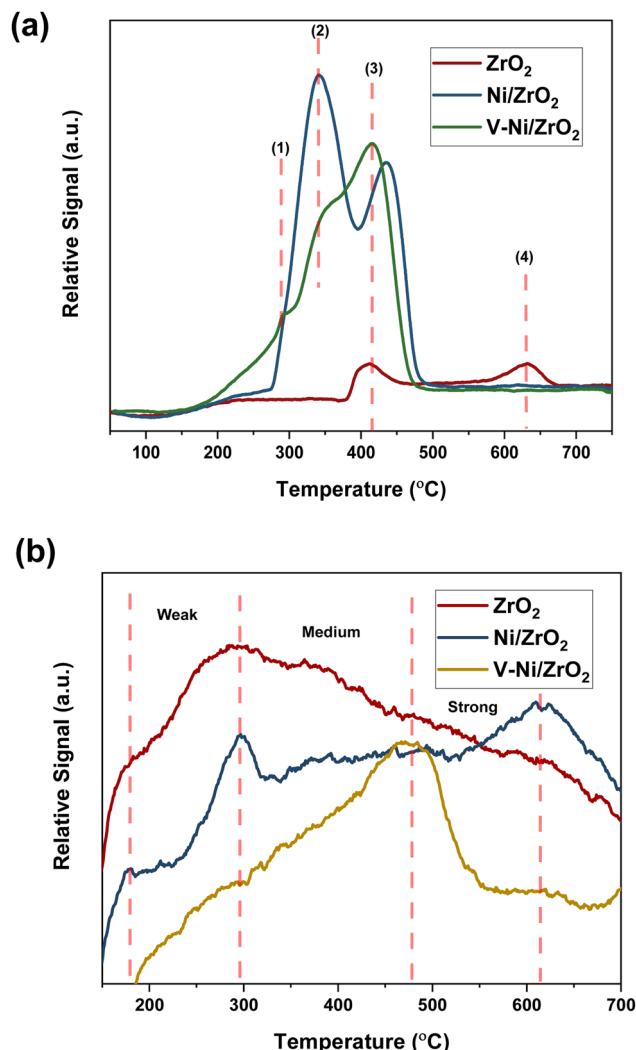
Fig. 3 Temperature programmed (a) hydrogen reduction and (b) ammonia desorption of ZrO_2, Ni/ZrO_2 and $V–Ni/ZrO_2$.

the support and the strong acid sites of the active Ni phase. The catalyst modification with vanadia resulted in a desorption peak at roughly 470 °C, which indicates medium-to-strong acidity. The reduction in NH_3-desorption temperature after V addition is due to increased oxygen vacancies and decreased acidic Ni sites on the zirconia surface (lower Ni wt%).[57] This influenced catalytic performance, as strong acidic sites are known to boost catalytic activity in deoxygenation reactions but may also cause catalyst deactivation and promote bio-hydrocarbon cracking.[58] Medium acidity catalysts are preferred as they enhance selectivity and conversion while inhibiting bio-hydrocarbon cracking.[59]

The XPS spectra (Fig. 4) provide detailed insights into the elemental composition and oxidation states of the nanomaterials. The Zr 3d region exhibits doublets in the 189–177 eV binding energy range: 182.2 and 184.6 eV (ZrO_2), 182.0 and 184.4 eV (Ni/ZrO_2), and 182.0 and 184.2 eV ($V–Ni/ZrO_2$). These values suggest the presence of a Zr^{4+} oxidation state and metal-to-support electronic interactions, as evidenced by the binding energy shifts following active phase dispersion.[60]

The O 1s spectra reveal a distinct lattice oxygen peak at 530 eV for all three oxides.[61] Notably, a shoulder peak at 533.2 eV indicates the formation of oxygen vacancies due to V_2O_5 incorporation. These vacancies are critical in enhancing catalytic activity by facilitating reactant adsorption.

Following Ni impregnation on the zirconia support, the Ni $2p_{3/2}$ binding peaks were identified at 856.2 eV and 855.8 eV for Ni/ZrO_2 and $V–Ni/ZrO_2$, respectively, corresponding to NiO and corroborating the PXRD assigned oxidation state for the active species.[62] Satellite peaks detected at 862.6 eV and 861.2 eV further confirm the presence of Ni^{2+} species.[63] Interestingly, adding vanadia to the catalyst surface reduces Ni^{2+} to metallic Ni^0, highlighting a modification of the surface chemistry. This change suggests strong interactions between Ni, V, and ZrO_2, enhancing the catalyst's deoxygenation performance by improving hydrogen activation and electron transfer processes.[59]

The binding energy peak assigned to V $2p_{3/2}$ is identified at 517.2 eV and corresponds to the presence of the V^{5+} species.[64]

3.2. Deoxygenation of fatty acid feedstock

To achieve high conversion and selectivity, fatty acid upgradation through deoxygenation can be tailored using different reaction parameters. The composition of the raw materials of fatty acid feeds utilized in this study is displayed in Table 2.

3.2.1. Evaluation of optimum reaction conditions. Temperature and time parameters are crucial in determining the conversion rate and product distribution in deoxygenating fatty carboxylic acids.[43] The optimum deoxygenation reaction conditions to produce bio-hydrocarbons over Ni/ZrO_2 were determined using TOFA as the model feedstock, containing C_{18} fatty acids, a major component of naturally occurring lipids.[65] Time-based experiments were carried out over 1 to 5 hours at 300 °C (Fig. 5a); the conversion ranged from a minimum of 12% after 1 h to a maximum of 61% after 5 h reaction times. The catalyst is most productive at 3 h reaction time as seen through the highest turnover frequency (TOF) of 105 h^{-1} at 3 h, after which a decline to 95 h^{-1} at 4 h and 86 h^{-1} at 5 h is observed. This reduction suggests a progressive decrease in available active sites, likely caused by surface blocking or catalyst coking over time.[66] Bio-hydrocarbon selectivity at the 5 hours mark was just 1.4% n-heptadecane, meaning very little direct decarboxylation to C_{17} bio-hydrocarbons occurs, and no further cracking of n-heptadecane to $C_{12}–C_{16}$ bio-hydrocarbons occurred. TOFA is first converted to stearic acid (67%), which, in turn, is consumed gradually over 1 h to 5 h, indicating that the reaction pathway involves prior hydrogenation of unsaturated fatty acids in TOFA at 300 °C. This is followed by ketonization of stearic acid with acetic acid to give 2-nonadecanone (26%) in 5 h. However, further decarbonylation of 2-nonadecanone to C_{18} bio-hydrocarbons was not observed under these conditions.[67]

To assess the effect of reaction temperature, the reaction was carried out at 25 °C increments starting from 250 °C to 350 °C (Fig. 5b). A steady increase in TOFA conversion with catalyst productivity is seen with an increase in temperature from 250 °C to 350 °C, with conversion reaching 80% and a TOF of 112
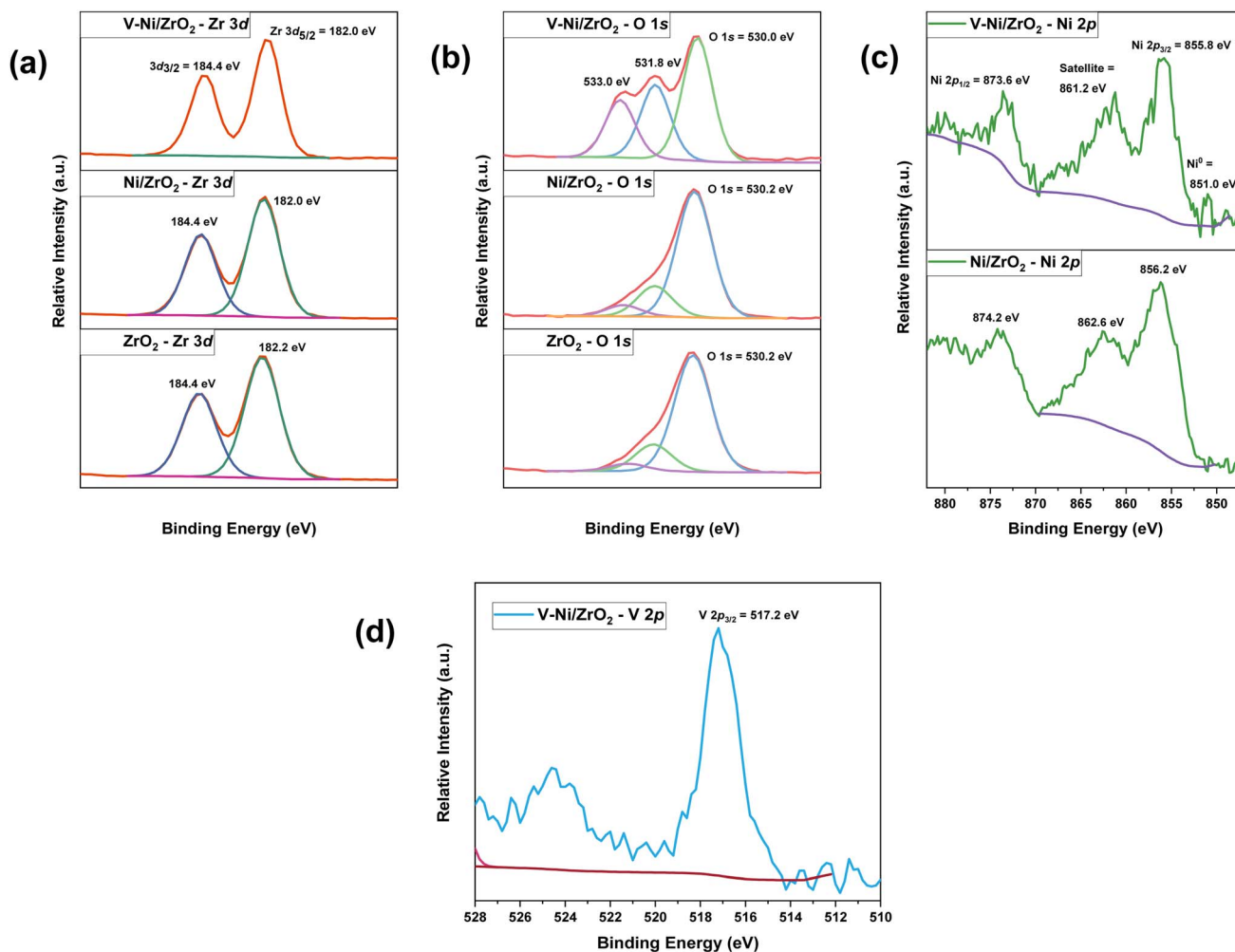
Fig. 4 XPS binding energy spectra of oxidic catalysts, showing (a) 3d, (b) O 1s, (c) Ni 2p, and (d) V 2p regions.

h^{-1}. The TOF increase with rising temperature confirms that the reaction rate is temperature-dependent.[68,69] At 250 °C, TOFA conversion reached 36%; however, no C_{17} or C_{18} bio-hydrocarbons or ketones were formed. Instead, the hydrogenation of unsaturated fatty acids in TOFA resulted in 100% selectivity to stearic acid. A shift in the reaction pathway to ketonization occurred at 325 °C, marked by the production of 2-nonadecanone (28%) and minute amounts of C_{18} bio-hydrocarbons (0.3% yield). A higher conversion rate of 80%, along with bio-hydrocarbon selectivities of 6.1% for C_{17} and 2.7% for C_{18}, were achieved at 350 °C, however, the increased operating

temperature also resulted in cracking of bio-hydrocarbons to shorter-chain products, C_{12}–C_{16} (1.6%).

The impact of the catalyst load was investigated to determine the optimum amount. Increasing the catalyst load provides more active sites, potentially improving the performance while reducing the number of available Ni active sites, which could hinder the hydrogenation of the unsaturated feedstock, leading to surface coking and catalyst deactivation.[70] Under the optimized reaction conditions of 350 °C/5 h, adding 5 mg of catalyst resulted in 68% conversion, with a 10.5% yield of C_{17} bio-hydrocarbons and a 5.1% yield of shorter alkanes produced *via*

Table 2 Fatty acid composition of the oleo-feedstock[a]

Feedstock	Palmitic acid (%)	Stearic acid (%)	Oleic acid (%)	Linoleic acid (%)	Linolenic acid (%)
TOFA	0.1	2.5	47.2	32.8	2.7
DCOFA	1.7	1.0	—	88.8	—
PO	40.5	—	20.7	—	—
WCO	15.1	0.3	33.9	22.4	28.2
Biodiesel	15.5	6.6	34.9	39.2	—

[a] TOFA: tall oil fatty acid; DCOFA: dehydrated castor oil fatty acid; PO: palm oil; WCO: waste cooking oil.
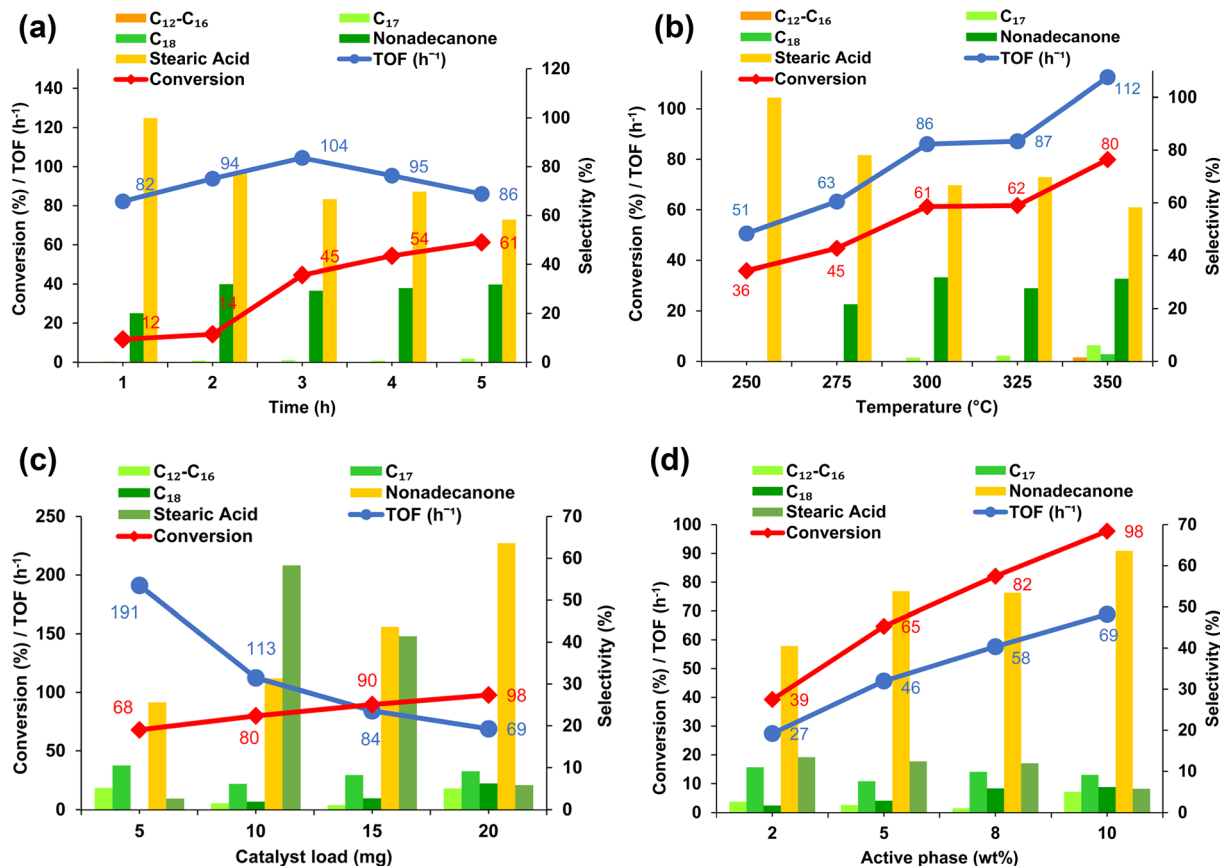
Fig. 5 (a) Optimization of TOFA ketonic decarboxylation by adjusting the reaction time (h). Conditions: TOFA (0.87 mmol), 10 wt% NiZrO$_2$ (10 mg), hexane (3 mL), acetic acid (1.8 mmol), FA (2.5 mmol), 300 °C, 800 rpm. (b) Optimization of TOFA ketonic decarboxylation by adjusting the temperature (°C). Reaction conditions: TOFA (0.87 mmol), 10 wt% NiZrO$_2$ (10 mg), hexane (3 mL), acetic acid (1.8 mmol), FA (2.5 mmol), 5 h, 800 rpm. (c) Optimization of TOFA ketonic decarboxylation by varying the catalyst loading. Reaction conditions: TOFA (0.87 mmol), 10 wt% NiZrO$_2$, hexane (3 mL), acetic acid (1.8 mmol), FA (2.5 mmol), 350 °C, 5 h, 800 rpm. (d) Optimization of TOFA ketonic decarboxylation by the active phase content (wt%). Reaction conditions: TOFA (0.87 mmol), cat. (20 mg), hexane (3 mL), acetic acid (1.8 mmol), FA (2.5 mmol), 350 °C, 5 h, 800 rpm.

hydrocracking (Fig. 5c). The cross-ketonization of TOFA with acetic acid remained low at 36%, highlighting the role of nickel particles in the decarboxylative-dehydration of unsaturated fatty acid. This limited activity may be a result of reduced active sites that decrease hydrogenation capacity, as evidenced by minimal yields of stearic acid. An increase in acidic sites on the catalyst surface encourages the deoxygenation of fatty acids by facilitating the C–O bond cleavage.[71] This is evidenced by the increased TOFA conversion, exceeding 90% with catalyst loadings of 15 mg and 20 mg. The optimal catalyst load was determined to be 20 mg (Fig. 5c), resulting in bio-hydrocarbon selectivities of 9.1% for C$_{17}$ and 6.2% for C$_{18}$, along with 63.6% ketone formation and a reduction in stearic acid yield to approximately 6%. This suggests that increasing the catalyst loading introduces enhanced catalytic activity *via* the acid–base sites of NiO and ZrO$_2$ that facilitate the sequential steps of hydrogenation → ketonization → decarbonylation → hydrogenation.[72,73]

The highest TOF was observed with 5 mg NiO/ZrO$_2$ loading (191 h^{-1}) (Fig. 5c). Notably, an increase in catalyst loading resulted in a decline in TOF values, indicating that at lower catalyst loading, all available active sites are effectively utilized

in the reaction, whereas higher catalyst loadings may introduce constraints such as mass transfer limitations.[72,73]

To further highlight the influence of active site density on the extent of ketonization, the Ni active phase was reduced to 2 wt%, 5 wt%, and 8 wt%. The 2 wt% Ni catalyst exhibited low fatty acid conversion (39%), demonstrating the significance of the acidic Ni sites in promoting formic acid dehydrogenation, feedstock hydrogenation, and facilitating deoxygenation. Increasing the Ni content to 5 wt% and 8 wt% led to improved fatty acid conversions of 65% and 82%, respectively, demonstrating enhanced deoxygenation and ketonization efficiency. A decrease in active NiO sites on the ZrO$_2$ surface limits the number of reactant molecules that can be converted into the desired deoxygenation products, emphasizing the crucial role of available active sites. This is evident from the observed increase in TOF as the number of active NiO sites on the ZrO$_2$ surface increases (Fig. 5d).

Under optimum conditions (350 °C/5 h), using 20 mg of 10 wt% Ni/ZrO$_2$, the major product shifted from stearic acid to nonadecanone (64%). Although the catalyst remained active, it produced hydrocarbon yields of around 20%. This result is expected given TOFA's highly unsaturated nature, which leads to

catalyst deactivation over time. As noted earlier, an initial hydrogenation step could promote ketonization and decarbonylation. Pre-hydrogenation of the double bonds in raw fatty acid feedstock to generate stearic acid may be required to enhance catalyst performance.[74]

The self-ketonization of individual feedstocks, such as fatty acids and acetic acid, can occur under similar reaction conditions, leading to valuable products.[75,76] Notably, the self-ketonization of C_{18} fatty acid and acetic acid is expected to yield key compounds like 17-pentatriacontane and acetone. However, the presence of these two compounds could not be distinctly assigned on the GC spectra, likely due to overlapping with the solvent, their presence in low concentrations, or, in the case of 17-pentatriacontanone, its high boiling point may prevent volatilization in the GC injector. Nevertheless, ^1H NMR analysis of product overlays at 250, 300, and 350 °C over 5 hours revealed two distinct singlets corresponding to the methyl group of acetone (2.18 ppm) and nonadecanone (2.14 ppm), attributed to differences in the electronic environment around the carbonyl groups (Fig. S4†). Additionally, the α-C of the methylene peak in nonadecanone appears as a multiplet at 2.42 ppm.[77] The presence of 17-pentatriacontene was later confirmed in the study via GC-MS, suggesting self-ketonization of TOFA. These findings highlight the versatility and commercial potential of this catalytic system, suggesting that with further optimization, it could serve as an efficient platform for sustainable ketone production. One of the carboxylic acids can be added in excess to promote self-ketonization over cross-ketonization.

3.2.2. Promoter effect and substrate evaluation.
A separate catalyst is often utilized to further convert the ketone product into bio-hydrocarbons, extending the deoxygenation reaction into a multi-step process.[21] However, the same catalyst can streamline the reaction into a single step, making the refinery system more economical. The presence of C═C bonds in the feedstock can accelerate catalyst deactivation through side reactions.[21] This is demonstrated by the predominant formation of stearic acid due to formic acid-mediated hydrogenation of the unsaturated oleic and linoleic acid in TOFA. To further promote the deoxygenation of the generated ketone, 10 bar gaseous hydrogen (H_2) was added to aid in the pretreatment of the unsaturated feed affording saturated stearic acid. This led to an enhanced bio-hydrocarbon selectivity, with 20.2% for C_{17}

(from 9.1%) and a marginal 7.7% selectivity to C_{18} (up from 6.2%).

The promotional effect of vanadia was also assessed under identical reaction conditions, demonstrating enhanced activity with 94% conversion and bio-hydrocarbon selectivity of 6.0% for C_{12}–C_{16}, 30.2% for C_{17}, and 9.4% for C_{18}. Notably, the introduction of vanadia led to an increase in TOF despite a reduction in the available NiO from 10 wt% to 8 wt%, highlighting its positive role as a promoter.[78] The incorporation of V_2O_5 into the catalyst improved Ni dispersion, partially reduced NiO to metallic Ni (Ni^0) (indicating strong metal–support interactions), and facilitated a synergistic effect between Ni and V. This synergy contributed to well-balanced acid–base properties, as evidenced by NH_3-TPD and XPS analyses, which are recognized for enhancing the deoxygenation of carboxylic acids.[79,80] Thus, the increased dispersion of Ni active sites and the availability of metallic Ni (enhanced by V-promotion), facilitate more efficient H_2 dissociation. Additionally, the oxophilic sites on ZrO_2 contribute to increased catalytic activity, promoting the deoxygenation of fatty acids to produce bio-hydrocarbons.[37] This was validated by conducting the reaction under the same conditions using unsupported NiO and ZrO_2 support, which primarily yielded fatty alcohols and fatty ketones, respectively (Fig. S5 and S6†).

A single concentration of vanadium (1.5 wt%), selected based on the literature,[81] was employed for the study at this time to simplify the analysis and assess whether the V–Ni/ZrO$_2$ catalyst system enhances ketonization of TOFA and related raw fatty acid feedstock. However, optimizing the vanadia-to-nickel loading ratio to achieve a vanadia surface density within the monolayer coverage range could enhance catalyst performance and efficiency by favouring the ketonization–decarbonylation pathway over decarboxylation.[82]

Subsequently, various feedstocks were evaluated using the modified V–Ni/ZrO$_2$ catalyst to investigate the influence of carbon chain length and degree of saturation on product yield and selectivity (Table 3). The substrate scope included dehydrated castor oil fatty acid (DCOFA), palm oil (PO), WCO, and FAME (biodiesel). When replacing TOFA with DCOFA, which predominantly consists of linoleic acid – $C_{18:2}$ – bio-hydrocarbon selectivity decreased to ∼25%. This decline is likely due to the higher degree of unsaturation in the feedstock, which can

Table 3 Conversion and selectivity for the deoxygenation of raw biomass feedstock[a]

| Substrate | % Conv. | % selectivity | | | | | Stearic acid | TOF (h^{-1}) |
		C_{12}–C_{16}	C_{17}	C_{18}	C_{19} nonadecanone	C_{12}–C_{19} bio-hydrocarbons		
TOFA[b]	92.6	5.1	9.1	6.2	63.6	84.0	5.8	69
TOFA[c]	89.9	3.0	20.2	7.7	2.3	33.2	7.9	63
TOFA	94.1	6.0	30.2	9.4	5.0	50.6	0.7	75
DCOFA	92.9	5.0	11.8	9.0	3.2	29.0	1.8	74
PO	62.7	23.3	14.8	12.1	23.8	74.0	—	50
WCO	88.5	31.3	5.8	1.2	12.6	50.9	—	71
FAME	71.5	5.0	4.0	1.9	11.3	22.2	3.1	57

[a] Reaction conditions: temperature – 350 °C, time – 5 h, substrate – 0.87 mmol, hydrogen source – FA (2.5 mmol) and H_2 (10 bar), and V–Ni/ZrO$_2$ (20 mg). [b] Without molecular hydrogen over the Ni/ZrO$_2$ catalyst. [c] Over the Ni/ZrO$_2$ catalyst. Conv. = conversion. Other products: Fatty alcohols, nonadecane, and stearic acid self-ketonization products (18-pentatriacontanone).

promote side reactions such as polymerization, leading to coking and catalyst deactivation.[83] Palm oil, comprising 40% saturated C_{16} palmitic acid, achieved 50% bio-hydrocarbon selectivity and 24% ketone formation, further proving that saturated fatty acids favour cross-ketonization and further deoxygenation. Finally, WCO and biodiesel produced 38% and 11% C_{12}–C_{18} bio-hydrocarbons, respectively, with conversion rates exceeding 70%.

Feedstock with varying carbon chain lengths and different functional groups to fatty carboxylic acids, such as carbonyl esters and triglycerides, may exhibit different reaction behaviours.[84,85] In this study, the higher degrees of DCOFA unsaturation resulted in lower bio-hydrocarbon yield, which can be attributed to side reactions that are reported to take place, such as radical formation or activation of the unsaturated molecules, which could promote oligomerization and coking.[76,86] In contrast, feedstocks with higher saturation levels, such as palm oil, favoured the ketonization/decarbonylation–hydrogenation pathway, yielding primarily C_{15}–C_{18} bio-hydrocarbons as well as octadecanol and C_{19} ketone.[21,87] Waste cooking oil predominantly promoted bio-hydrocarbon cracking, producing mainly pentadecane and, in smaller amounts – heptadecane. Deoxygenation of ester groups, such as biodiesel, typically occurs via the formation of carboxylic acid intermediates, which then undergo further deoxygenation to yield alkanes.[88,89] However, this additional reaction step likely requires higher energy input, contributing to the lower bio-hydrocarbon yields observed with biodiesel.

These findings highlight that the substrate composition significantly influences the reaction rate and product distribution. Lower carbon balances observed during the reactions suggest the occurrence of secondary reactions, such as oligomerization and polymerization, which form heavier molecules that may not be detected by gas chromatography (GC).[45]

3.3. Proposed reaction pathway

Scheme 2 illustrates the three reaction pathways observed in the ketonic decarboxylation catalyzed by Ni/ZrO_2 and $V–Ni/ZrO_2$. In pathway A, the formation of heptadecane is achieved via the elimination of CO_2 in the direct decarboxylation of stearic acid. This reaction pathway is the major route following the addition of molecular hydrogen. Alternatively, the C_{18} fatty acid feedstock cross-ketonizes with acetic acid to give nonadecanone ($C_{18}OC$), which can be further decarbonylated and hydrogenated to octadecane. This reaction pathway (B) reduces the oxygen content through the ejection of carbon dioxide and water and is a strategic method for replacing the carbon loss in catalytic decarboxylation. Finally, in pathway C, the fatty acid and acetic acid reactants may undergo self-ketonization, producing C_{35}-chain ketones that can be converted into pentatriacontane or acetone. Other products were observed in small amounts, such as the cracked bio-hydrocarbons (C_8–C_{14}) and decarbonylated alkenes (C_{17}).

In this work, the deoxygenation of TOFA over Ni/ZrO_2 without gaseous hydrogen favoured the cross-ketonization product (B) to yield ∼64% nonadecanone. The introduction of molecular hydrogen (H_2, 10 bar), combined with formic acid as a hydrogen donor, shifted the reaction pathway of the unsaturated feed (TOFA and DCOFA) to generate C_{17} bio-hydrocarbons
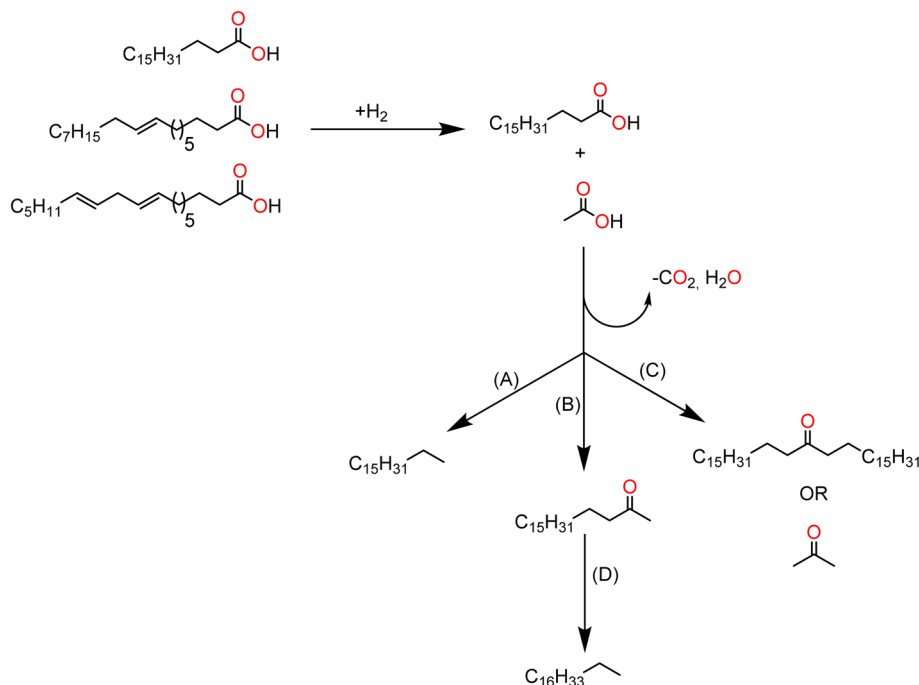
Scheme 2 Deoxygenation pathways of the hydrogenated crude fatty acids over Ni/ZrO_2 and $V–NiZrO_2$ catalysts. (A) Direct decarboxylation of C_{18} fatty acids yielding C_{17} bio-hydrocarbons, (B) cross-ketonization of acetic acid with C_{18} fatty acids yielding nonadecanone, (C) self-ketonization of acetic acid and C_{18} fatty acids, and (D) decarbonylation of nondecanone to C_{18} bio-hydrocarbon.

(*via* decarboxylation) as well as octadecane in minor amounts (*via* cross-ketonization). However, the observed lower carbon balance indicates that insufficient hydrogen addition may suppress the ketonization of unsaturated feedstock while leading to undesired polymerization and oligomerization reactions.[90]

To address this limitation, a two-step process involving the prehydrogenation of the unsaturated fatty acid feedstock followed by the ketonization–deoxygenation reaction could improve the bio-hydrocarbon yield and increase the carbon balance.[21] Additionally, increasing the availability of molecular hydrogen or enhancing the decomposition of the formic acid hydrogen donor through modifications to the catalysts' hydrogenation activity could minimize radical formation, promote substrate saturation, and subsequently enhance the ketonization pathway.[33]

3.4. Catalyst stability over time

Catalyst sintering and active phase agglomeration are common challenges in Ni-based catalytic deoxygenation systems. Adding a promoter can increase the uniformity of active phase dispersion by decreasing the particle size and enhancing the metal-to-support interactions. A study on TOFA deoxygenation using Ni/

ZrO_2 and V–Ni/ZrO_2 over 5, 10, and 15 h time frames highlighted the effect of vanadia modification on the performance of the Ni catalyst over time. The desired bio-hydrocarbons were generated with a conversion rate above 89% over both catalysts. Increasing the catalyst time beyond the 5 hours threshold improved the efficacy of both catalysts; nevertheless, the emergence of shorter-chain bio-hydrocarbons over the Ni/ZrO_2 catalyst signals catalyst deactivation over time at high temperatures. At 15 h (100% conversion), higher degrees of cracking bio-hydrocarbons and wide product distributions were examined with <C_{10} bio-hydrocarbons identified (Fig. 6). Interestingly, the V–Ni/ZrO_2 catalyst displayed increased production of C_{18} bio-hydrocarbon selectivity with time (~16%), indicating that the catalyst is still active after 15 h (Fig. 7). Octadecanol and nonadecanone were observed in significant quantities (~40% selectivity), indicating that the reaction favours ketonization over time. Other identified products (*via* GC-MS) include octadecene, nonadecene, and 17-pentatriacontene, indicating alternative reaction pathways such as decarbonylation, hydrodeoxygenation, and self-ketonization (Fig. S7†). The addition of V_2O_5 to the catalyst structure resulted in greater nickel dispersion, improved structural stability (*via* strong metal–support interactions), and an optimal combination of the acidic nature of Ni and the redox properties of V, yielding well-balanced acid–
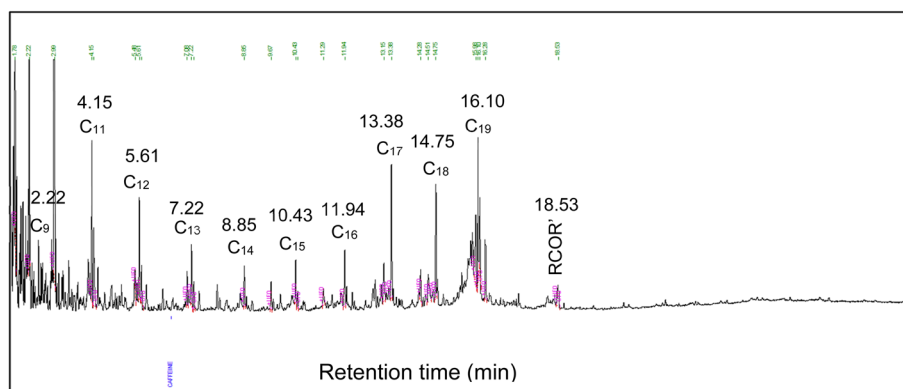

Fig. 6 Ni/ZrO_2-catalysed deoxygenation products at 15 h, showing green diesel (C_{11}–C_{18}), some green gasoline (C_9) bio-hydrocarbons, and fatty ketone product distribution.
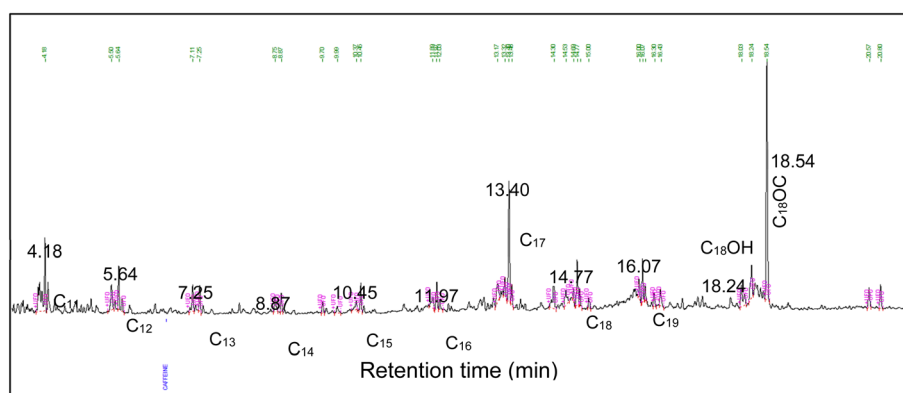

Fig. 7 V–Ni/ZrO_2-catalysed deoxygenation products at 15 h, showing green diesel range bio-hydrocarbon, fatty alcohol and fatty ketone product distribution.
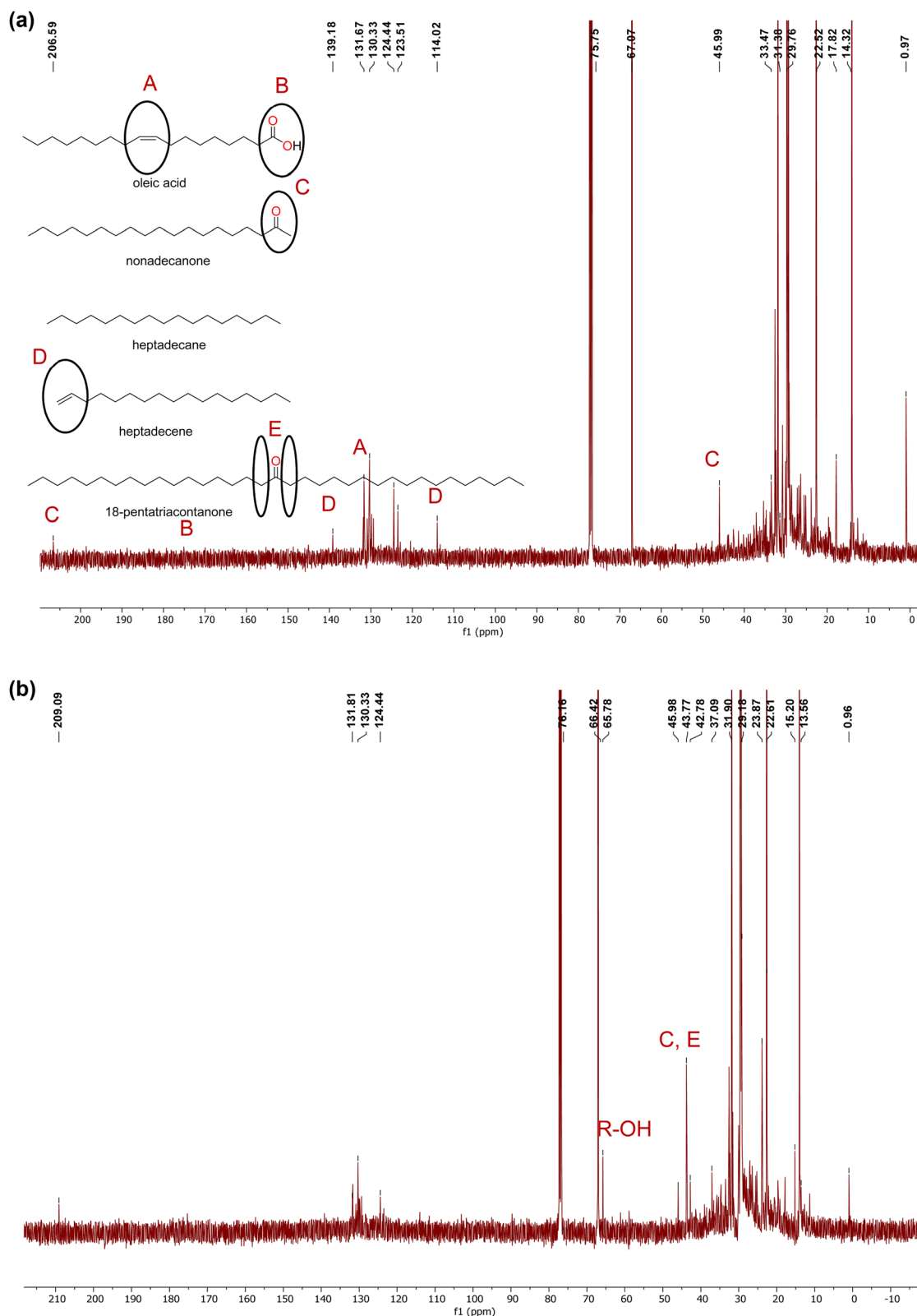
Fig. 8 $^{13}C\{^1H\}$ NMR spectra of the deoxygenation products over (a) NiZrO$_2$ and (b) V–Ni/ZrO$_2$ catalysts.

base characteristics that are favourable for the deoxygenation of carboxylic acids.[79,80] These selectivity changes reveal active site modifications (such as surface poisoning and reconstruction)

influence TOFA conversion and product yield. Additional characterization using $^{13}C\{^1H\}$ NMR confirmed the formation of ketone bio-hydrocarbons over the Ni/ZrO$_2$ and V–Ni/ZrO$_2$ at

$\delta = 206.6$ ppm and 209.1 ppm (C), respectively. The vanadia-promoted deoxygenation reaction also signals the presence of fatty alcohol with a signal at 65.8 ppm (which is not observed over the unmodified nickel catalyst). Interestingly, the less selective nature of the Ni/ZrO$_2$ catalyst is made clear by the multiple olefin signals in the range 139–114 ppm, indicating that side reactions like isomerization, decarbonylation, and possible cyclization occur (Fig. 8).

4. Conclusion

In this paper, we demonstrate the effective ketonic decarboxylation ability of the vanadia-modified Ni/ZrO$_2$ catalyst. The cross-ketonization of fatty acid feedstock with acetic acid exhibited 64% selectivity for 2-nonadecanone at optimum 350° C/5 h using formic acid as a hydrogen carrier. Initially, low hydrocarbon selectivity was observed due to the high degree of unsaturation in the raw material.[91] The addition of minimal molecular hydrogen (10 bar) to aid formic acid in the hydrogenation and subsequent ketonization of the substrate improved selectivity towards C$_{17}$ (20.2% mole yield) and C$_{18}$ bio-hydrocarbons (7.7% mole yield). The addition of a V$_2$O$_5$-promoter to the Ni/ZrO$_2$ catalyst resulted in a reduction in the active phase particle size and an improvement in Ni dispersion, ultimately leading to higher bio-hydrocarbon selectivity (C$_{17}$ = 30.2%; C$_{18}$ = 9.4%). This is attributed to the synergy between the enhanced Ni acid sites and high oxygen vacancies on the vanadia surface, generating a durable effective catalyst.

The influence of the fatty acid degree of saturation and chain length on the catalyst performance was evaluated. Enhanced bio-hydrocarbon selectivity was observed over the more saturated palm oil substrate. In contrast, highly saturated fatty acid feed (e.g., DCOFA and TOFA) led to decarboxylation and suggested side reactions such as polymerization. Catalyst stability testing was also carried out by increasing the reaction time and observing the product distribution at different intervals; Ni/ZrO$_2$ displayed high conversion, although the selectivity was compromised, resulting in the appearance of cracking products. Inversely, the V-promoted catalyst increased C$_{18}$ selectivity and ketonization by-products.

These findings suggest that a pre-hydrogenation treatment influences the deoxygenation of unsaturated crude fatty carboxylic acids. The reaction typically favours the decarboxylation pathway, which affords lower energy-dense carbon chains (C$_{n-1}$). At low catalyst loads (<10 wt%), the cross-ketonization of fatty acid feedstock with readily available and cost-effective acetic acid is a promising method for generating C$_{18}$ (via keto-nization–decarbonylation) and C$_{19}$ bio-hydrocarbons (via keto-nization–hydrodeoxygenation), as well as fatty ketones and fatty alcohols that can be applied in jet fuel, biodiesel, and lubricant production. Furthermore, vanadium incorporation into the catalyst structure enhances Ni dispersion and increases the density of oxygen vacancy sites, thereby improving deoxygenation efficiency and catalyst stability. Other notable reaction products include the self-ketonization of tall oil fatty acids (TOFAs) to produce 17-pentatriacontene, a high-value component in lubricant applications, and the self-ketonization of

acetic acid to generate acetone, an essential solvent and industrial chemical.

While the products are distributed between bio-hydrocarbons, fatty ketones, and fatty alcohols, optimizing the vanadia loading to achieve monolayer coverage and increasing the Ni loading could promote bio-hydrocarbon production. Varying the Ni-to-V ratio could also improve ketone formation, as well as subsequent decarbonylation (to give C$_{18}$) and hydrogenation (to give C$_{19}$). The synergy between the inexpensive vanadium and nickel shows promise as an industrial deoxygenation catalyst. Further optimization of the catalyzed ketonization process promises economically viable products with valuable outputs.

Data availability

The authors confirm that all data supporting the findings of this study are provided within the article and its ESI.† Any additional information will be provided upon request.

Author contributions

Sibongile Pikoli: conceptualization, methodology, validation, formal analysis, investigation, writing – original draft, writing – review & editing, visualization, project administration. Avela Kunene: conceptualization, methodology, formal analysis, co-supervision. Banothile Makhubela: conceptualization, methodology, resources, writing – review and editing, visualization, supervision, funding acquisition.

Conflicts of interest

There are no conflicts to declare.

Acknowledgements

References

1 W. H. L. Stafford, G. A. Lotter, G. P. von Maltitz and A. C. Brent, *Dev. South. Afr.*, 2019, **36**, 155–174.

2 B. Karmakar and G. Halder, *Energy Convers. Manag.*, 2019, **182**, 307–339.

3 Y. Zhou, J. Remón, Z. Jiang, A. S. Matharu and C. Hu, *Green Energy Environ.*, 2023, **8**, 722–743.

4 M. Z. Hossain, M. B. I. Chowdhury, A. K. Jhawar, W. Z. Xu, M. C. Biesinger and P. A. Charpentier, *ACS Omega*, 2018, **3**, 7046–7060.

5 J. M. Crawford, C. S. Smoljan, J. Lucero and M. A. Carreon, *Catalysts*, 2019, **9**, 42.

6 A. I. Tsiotsias, S. Hafeez, N. D. Charisiou, S. M. Al-Salem, G. Manos, A. Constantinou, S. AlKhoori, V. Sebastian, S. J. Hinder, M. A. Baker, K. Polychronopoulou and M. A. Goula, *Renew. Energy*, 2023, **206**, 582–596.

7 N. Aliana-Nasharuddin, N. Asikin-Mijan, G. Abdulkareem-Alsultan, M. I. Saiman, F. A. Alharthi, A. A. Alghamdi and Y. H. Taufiq-Yap, *RSC Adv.*, 2019, **10**, 626–642.

8 S. Liu, T. Simonetti, W. Zheng and B. Saha, *ChemSusChem*, 2018, **11**, 1446–1454.

9 D. Jiraroj, O. Jirarattanapochai, W. Anutrasakda, J. S. M. Samec and D. N. Tungasmita, *Appl. Catal., B*, 2021, **291**, 120050.

10 Y. Liu, K. E. Kim, M. B. Herbert, A. Fedorov, R. H. Grubbs and B. M. Stoltz, *Adv. Synth. Catal.*, 2014, **356**, 130–136.

11 P. A. Zharova, A. V. Chistyakov, S. S. Shapovalov, A. A. Pasynskii and M. V. Tsodikov, *Energy*, 2019, **172**, 18–25.

12 S. Janampelli and S. Darbha, *Energy Fuels*, 2018, **32**, 12630–12643.

13 M. Toba, Y. Abe, H. Kuramochi, M. Osako, T. Mochizuki and Y. Yoshimura, *Catal. Today*, 2011, **164**, 533–537.

14 M. F. Wagenhofer, E. Baráth, O. Y. Gutiérrez and J. A. Lercher, *ACS Catal.*, 2017, **7**, 1068–1076.

15 A. Zheng, Z. Huang, G. Wei, K. Zhao, L. Jiang, Z. Zhao, Y. Tian and H. Li, *iScience*, 2020, **23**, 100814.

16 S. Shylesh, L. A. Bettinson, A. Aljahri, M. Head-Gordon and A. T. Bell, *ACS Catal.*, 2020, **10**, 4566–4579.

17 M. Renz, *Eur. J. Org. Chem.*, 2005, 979–988.

18 S. Wang and E. Iglesia, *J. Catal.*, 2017, **345**, 183–206.

19 E. Heracleous, D. Gu, F. Schüth, J. A. Bennett, M. A. Isaacs, A. F. Lee, K. Wilson and A. A. Lappas, *Biomass Convers. Biorefin.*, 2017, **7**, 319–329.

20 A. Gumidyala, T. Sooknoi and S. Crossley, *J. Catal.*, 2016, **340**, 76–84.

21 K. Lee, M. Y. Kim and M. Choi, *ACS Sustain. Chem. Eng.*, 2018, **6**, 13035–13044.

22 A. C. Rustan and C. A. Drevon, *Encyclopedia of Life Sciences*, 2005, pp. 1–7.

23 V. Kostik, S. Memeti and B. Bauer, *J. Hyg. Eng. Des.*, 2013, **4**, 112–116.

24 S. P. Pyl, T. Dijkmans, J. M. Antonykutty, M. F. Reyniers, A. Harlin, K. M. Van Geem and G. B. Marin, *Bioresour. Technol.*, 2012, **126**, 48–55.

25 J. Mikulec, A. Kleinová, J. Cvengroš, L. Joríková and M. Banič, *Int. J. Chem. Eng.*, 2012, **2012**, 1–9.

26 G. Lawer-Yolar, B. Dawson-Andoh and E. Atta-Obeng, *Sustainable Chem.*, 2021, **2**, 206–221.

27 P. Mäki-Arvela, B. Rozmysłowicz, S. Lestari, O. Simakova, K. Eränen, T. Salmi and D. Y. Murzin, *Energy Fuels*, 2011, **25**, 2815–2825.

28 K. Jeništová, I. Hachemi, P. Mäki-Arvela, N. Kumar, M. Peurla, L. Čapek, J. Wärnå and D. Y. Murzin, *Chem. Eng. J.*, 2017, **316**, 401–409.

29 L. J. Konwar, B. Oliani, A. Samikannu, P. Canu and J. P. Mikkola, *Biomass Convers. Biorefin.*, 2022, **12**, 51–62.

30 T. N. Pham, T. Sooknoi, S. P. Crossley and D. E. Resasco, *ACS Catal.*, 2013, **3**, 2456–2473.

31 G. Pacchioni, *ACS Catal.*, 2014, **4**, 2874–2888.

32 T. N. Pham, D. Shi and D. E. Resasco, *Top. Catal.*, 2014, **57**, 706–714.

33 P. Promchana, A. Boonchun, J. T-Thienprasert, T. Sooknoi and T. Maluangnont, *Catal. Today*, 2021, **375**, 418–428.

34 H. Chen, X. Zhang, J. Zhang and Q. Wang, *Catal. Sci. Technol.*, 2018, **8**, 1126–1133.

35 S. Zulkepli, N. A. Rahman, H. Voon Lee, C. Kui Cheng, W. H. Chen and J. Ching Juan, *Energy Convers. Manag.*, 2022, **273**, 116371.

36 R. Kaewmeesri, J. Nonkumwong, T. Witoon, N. Laosiripojana and K. Faungnawakij, *Nanomaterials*, 2020, **10**, 1–15.

37 A. Pennetier, W. Y. Hernandez, B. T. Kusema and S. Streiff, *Appl. Catal., A*, 2021, **624**, 118301.

38 H. Ning, J. Deng, Z. Wang, L. Zhao, Z. Zhang, H. Liu, Z. Lan and J. Guo, *Int. J. Hydrogen Energy*, 2020, **45**, 28078–28086.

39 S. W. Jeon, I. Song, H. Lee and D. H. Kim, *Chemosphere*, 2021, **275**, 130105.

40 K. Świrk, P. Summa, D. Wierzbicki, M. Motak and P. Da Costa, *Int. J. Hydrogen Energy*, 2021, **46**, 17776–17783.

41 I. T. Ghampson, G. Pecchi, J. L. G. Fierro, A. Videla and N. Escalona, *Appl. Catal., B*, 2017, **208**, 60–74.

42 I. L. Simakova and D. Y. Murzin, *J. Energy Chem.*, 2016, **25**, 208–224.

43 Y. Zhou, X. Liu, P. Yu and C. Hu, *Fuel*, 2020, **278**, 118295.

44 C. S. Smoljan, J. M. Crawford and M. A. Carreon, *Catal. Commun.*, 2020, **143**, 106046.

45 M. López, R. Palacio, S. Royer, A. S. Mamede and J. J. Fernández, *Microporous Mesoporous Mater.*, 2020, **292**, 109694.

46 P. Sinha, A. Datar, C. Jeong, X. Deng, Y. G. Chung and L. C. Lin, *J. Phys. Chem. C*, 2019, **123**, 20195–20209.

47 A. M. Predescu, E. Matei, A. C. Berbecaru, M. Râpă, M. G. Sohaciu, C. Predescu and R. Vidu, *Materials*, 2021, **14**, 2539.

48 U. Rashid and F. Anwar, *Fuel*, 2008, **87**, 265–273.

49 A. Demirbas, *Energy Convers. Manag.*, 2009, **50**, 923–927.

50 J. P. Kanter, P. J. Honold, D. Lüke, S. Heiles, B. Spengler, M. A. Fraatz, C. Harms, J. P. Ley, H. Zorn and A. K. Hammer, *Appl. Microbiol. Biotechnol.*, 2022, 6095–6107.

51 G. J. S. Dawes, E. L. Scott, J. Le Nôtre, J. P. M. Sanders and J. H. Bitter, *Green Chem.*, 2015, **17**, 3231–3250.

52 A. Borodziński and M. Bonarowska, *Langmuir*, 1997, **13**, 5613–5620.

53 A. Gil, *Catal. Today*, 2023, **423**, 114016.

54 S. Benomar, A. Massó, B. Solsona, R. Issaadi and J. M. López Nieto, *Catalysts*, 2018, **8**, 126.

55 R. A. El-Salamony, S. A. El-Temtamy, A. M. A. El Naggar, S. A. Ghoneim, D. R. Abd El-Hafiz, M. A. Ebiad, T. Gendy and A. M. Al-Sabagh, *Int. J. Energy Res.*, 2021, **45**, 3899–3912.

56 Y. Shao, T. Wang, K. Sun, Z. Zhang, L. Zhang, Q. Li, S. Zhang, G. Hu and X. Hu, *Green Energy Environ.*, 2021, **6**, 557–566.

57 T. Viinikainen, H. Rönkkönen, H. Bradshaw, H. Stephenson, S. Airaksinen, M. Reinikainen, P. Simell and O. Krause, *Appl. Catal., A*, 2009, **362**, 169–177.

58 S. V. Sancheti, G. D. Yadav and P. K. Ghosh, *ACS Omega*, 2020, **5**, 5061–5071.

59 M. Gousi, C. Andriopoulou, K. Bourikas, S. Ladas, M. Sotiriou, C. Kordulis and A. Lycourghiotis, *Appl. Catal., A*, 2017, **536**, 45–56.

60 A. A. Shutilov, M. N. Simonov, Y. A. Zaytseva, G. A. Zenkovets and I. L. Simakova, *Kinet. Catal.*, 2013, **54**, 184–192.

61 J. Ni, W. Leng, J. Mao, J. Wang, J. Lin, D. Jiang and X. Li, *Appl. Catal., B*, 2019, **253**, 170–178.

62 D. Zeng, Y. Li, H. Ma, F. Cui and J. Zhang, *ACS Sustain. Chem. Eng.*, 2021, **9**, 15612–15622.

63 E. Puello-Polo, Y. P. Reales, E. Marquez, D. G. Larruded, L. C. C. Arzuza and C. A. T. Toloza, *Catal. Lett.*, 2021, **151**, 2038–2055.

64 X. Wang, Y. Kang, J. Li and D. Li, *Korean J. Chem. Eng.*, 2019, **36**, 650–659.

65 A. L. Cardoso, S. C. G. Neves and M. J. da Silva, *Energies*, 2008, **1**, 79–92.

66 B. Rozmysłowicz, P. Mäki-Arvela, A. Tokarev, A. R. Leino, K. Eränen and D. Y. Murzin, *Ind. Eng. Chem. Res.*, 2012, **51**, 8922–8927.

67 M. Romero, A. Pizzi, G. Toscano, A. A. Casazza, G. Busca, B. Bosio and E. Arato, *Chem. Eng. Trans.*, 2018, **64**, 121–126.

68 A. Ramesh, P. Tamizhdurai, V. L. Mangesh, K. Palanichamy, S. Gopinath, K. Sureshkumar and K. Shanthi, *Int. J. Hydrogen Energy*, 2019, **44**, 25607–25620.

69 K. N. Papageridis, N. D. Charisiou, S. L. Douvartzides, V. Sebastian, S. J. Hinder, M. A. Baker, S. AlKhoori, K. Polychronopoulou and M. A. Goula, *Fuel Process. Technol.*, 2020, **209**, 106547.

70 M. Grilc and B. Likozar, *Chem. Eng. J.*, 2017, **330**, 383–397.

71 S. De, B. Saha and R. Luque, *Bioresour. Technol.*, 2015, **178**, 108–118.

72 L. Fu, Z. Liu, X. Li, Y. Li, H. Yang and Y. Liu, *Fuel*, 2022, **322**, 124027.

73 J. Wang, L. Xu, R. Nie, X. Lyu and X. Lu, *Fuel*, 2020, **265**, 116913.

74 D. R. Vardon, B. K. Sharma, H. Jaramillo, D. Kim, J. K. Choe, P. N. Ciesielski and T. J. Strathmann, *Green Chem.*, 2014, **16**, 1507–1520.

75 B. Smith, L. Li, D. D. Perera-Solis, L. F. Gildea, V. L. Zholobenko, P. W. Dyer and H. C. Greenwell, *Inorganics*, 2018, **6**, 121.

76 S. Zaidi, N. Asikin-Mijan, A. S. Hussain, M. S. Mastuli, F. A. Alharthi, A. A. Alghamdi and Y. H. Taufiq-Yap, *J. Taiwan Inst. Chem. Eng.*, 2021, **121**, 217–228.

77 N. Singh, M. Verma, D. Mehta and B. K. Mehta, *Indian J. Chem., Sect. B:Org. Chem. Incl. Med. Chem.*, 2005, **44**, 1742–1744.

78 W. Zhou, H. Xin, H. Yang, X. Du, R. Yang, D. Li and C. Hu, *Catalysts*, 2018, **8**, 15–18.

79 R. Loe, K. Huff, M. Walli, T. Morgan, D. Qian, R. Pace, Y. Song, M. Isaacs, E. Santillan-Jimenez and M. Crocker, *Catalysts*, 2019, **9**, 200.

80 M. F. Kamaruzaman, Y. H. Taufiq-Yap and D. Derawi, *Biomass Bioenergy*, 2020, **134**, 105476.

81 D. Le, N. Chaidherasuwet, A. Rueangthaweep, C. Kulsing and N. Hinchiranan, *Catal. Today*, 2021, **407**, 260–273.

82 S. Koust, B. N. Reinecke, K. C. Adamsen, I. Beinik, K. Handrup, Z. Li, P. G. Moses, J. Schnadt, J. V. Lauritsen and S. Wendt, *J. Catal.*, 2018, **360**, 118–126.

83 T. Morgan, E. Santillan-Jimenez, A. E. Harman-Ware, Y. Ji, D. Grubb and M. Crocker, *Chem. Eng. J.*, 2012, **189–190**, 346–355.

84 B. P. Pattanaik and R. D. Misra, *Renew. Sustain. Energy Rev.*, 2017, **73**, 545–557.

85 G. A. Alsultan, N. Asikin-Mijan, H. V. Lee, A. S. Albazzaz and Y. H. Taufiq-Yap, *Energy Convers. Manag.*, 2017, **151**, 311–323.

86 T. H. Kim, K. Lee, M. Y. Kim, Y. K. Chang and M. Choi, *ACS Sustain. Chem. Eng.*, 2018, **6**, 17168–17177.

87 Y. Liu, X. Yang, H. Liu, Y. Ye and Z. Wei, *Appl. Catal., B*, 2017, **218**, 679–689.

88 I. Kubickova, M. Snåre, K. Era, D. Y. Murzin, V. Uni, F. Turku, R. V September, V. Re, M. Recei and V. October, *Energy Fuels*, 2007, 30–41.

89 M. Žula, M. Grilc and B. Likozar, *Chem. Eng. J.*, 2022, **444**, 136564.

90 H. Chen, S. Yao, W. Lin, Z. Zhang, X. Hu, X. Liu, B. Yan, K. Chen, Y. Qin, Y. Zhu, X. Lu, P. Ouyang, J. Fu and J. G. Chen, *Chem. Eng. J.*, 2020, **390**, 124603.

91 S. A. Aleem, N. Asikin-Mijan, A. S. Hussain, C. H. Voon, A. Dolfi, S. Sivasangar and Y. H. Taufiq-Yap, *RSC Adv.*, 2021, **11**, 31972–31982.